EFFECT OF HEAT CAPACITY VARIATION ON HIGH-PERFORMANCE HEAT EXCHANGERS FOR THERMO-MECHANICAL ENERGY STORAGE

P. Farres-Antunez, A.J. White

Cambridge University Engineering Department (CUED)

Keywords: thermal energy storage; heat exchanger; pinch point; heat capacity variation; exergy analysis; optimisation.

Abstract

Counter-flow heat exchangers constitute a major component of several thermo-mechanical energy storage technologies. They are used to transfer thermal energy between the working fluid and the storage fluid, and exergy losses undergone during this process can affect significantly the efficiency of the whole system. The principal sources of loss are irreversible heat transfer and pressure losses, and optimisation is required to find the right balance between them. In this article we focus on the effect that the variation of the specific heat capacity of some fluids has on the thermal component of the loss. First, we assume a linear dependence of the heat capacity with temperature and study the problem analytically, showing that a minimum exergetic loss exists when the variation is different for the two fluids. The effect is negligible in low-performance heat exchangers but it is found to have a critical impact in high-performance devices with a very high number of transfer units. Second, the minimum loss for several couples of real fluids is computed numerically and compared with the prediction of the analytical model. Finally, the effect that this phenomenon has on the optimisation of a flat-plate, counter-flow heat exchanger is studied.

1 Introduction

Growing levels of renewable energy generation, particularly from wind and solar power projects, are raising the need for new large-scale electrical storage projects. Pumped hydro is widely regarded as the most mature and successful technology in the field, but its capability to continue expanding is often limited by geographic constraints, and in many countries the most adequate sites have already been exploited [1]. In this context, thermo-mechanical energy storage (TMS) systems are becoming increasingly interesting. Such systems embrace several technologies that are mechanically driven and store electricity, partially or completely, in the form of thermal energy. They include, among others:

1. Pumped thermal energy storage (PTES), in which a thermal energy potential is created between two insulated thermal reservoirs, via mechanical compression and expansion of a working fluid that transports heat between them. The system operates as a heat pump during charge and as a heat engine during discharge. Several PTES concepts have been proposed, including a system based on the closed Brayton cycle [2, 3] (which stores the energy as sensible heat) and a number of systems based on the Rankine cycle operating with different working fluids, such as water [4], ammonia [5], or supercritical CO_2 [6] (which store part of the energy as sensible heat and part as latent heat).

2. Liquid air energy storage (LAES), also known as cryogenic energy storage (CES), which liquefies atmospheric air and stores it at atmospheric pressure [7]. The liquefaction and recovery process also require storing energy as sensible heat, both above and below ambient temperature.

3. Compressed air energy storage (CAES), in its adiabatic version, which stores part of the energy as a thermal energy potential and another part as a pressure (mechanical) potential [8].

The heat exchanger (HEX) constitutes a major component of all these systems, except those that use solid storage media and direct heat transfer between the solid and the working fluid (such as in packed-bed reservoirs). The principal sources of loss are irreversible heat transfer and pressure losses, and a second-law analysis accompanied by geometrical optimisation is necessary to find the most adequate balance between them in exergetic terms [9]. Several authors have approached this problem in the past, particularly in the context of gas-to-gas recuperators and cryogenic applications. The counter-flow design is normally selected in such works, as it provides the highest effectiveness for a given number of transfer units (NTU) and matching heat capacity rates [10], and is therefore the most effective in minimizing irreversible heat transfer. A number of non-dimensional parameters have been proposed to evaluate the rate of entropy generation [11] (this being proportional to the rate of exergy loss), and analytical solutions have been developed assuming either perfect gas behaviour or constant liquid properties [12]. In some TMS applications, however, the temperature difference between the two ends of the HEX is sufficiently large for the variation of the thermophysical properties of the fluids to be non-negligible.

When real properties are accounted for, one can observe that the variation of the specific heat capacity of some fluids gives rise to pinch points that force irreversible heat transfer. While pinch point issues are well known in heat exchangers where one stream undergoes a phase change and the other does not, in this article we focus our attention to heat exchangers operating with single-phase fluids and analyse the effect that the variation of the specific heat capacity has on the thermal component of the exergetic loss.

We start by selecting a non-dimensional index which describes the exergy performance of the HEX and which is meant to be particularly suitable for TMS systems. Next, we assume a linear dependence of the heat capacity with temperature and use this index to show that a minimum exergetic loss emerges when the variation is different for the two fluids. The effect is found to be negligible for heat exchangers with a low number of transfer units, but becomes very relevant for high-performance devices. Following this, several couples of fluids are taken as examples to evaluate the minimum loss. Results of the analytical linear approximation are compared with a numerical approach which allows the study of more complex dependencies. Finally, a computational model of a flat-plate, counter-flow HEX is used to show the effect that such pinch points have on the optimisation process.

2 Analytical study

2.1 Exergy loss in heat exchangers and non-dimensionalisation

We start by applying the steady-flow entropy equation to a small section of a heat exchanger, as shown in Figure 1, where the two fluid streams exchange heat but the heat transfer to the environment is negligible (as the HEX is assumed to be thermally insulated):

$$\mathrm{d}\dot{S}_{irr} = \dot{m}_A\,\mathrm{d}s_A + \dot{m}_B\,\mathrm{d}s_B \tag{1}$$

Separating ds in its temperature and pressure differential components,

$$\mathrm{d}s = \left(\frac{\partial s}{\partial T}\right)_p \mathrm{d}T + \left(\frac{\partial s}{\partial p}\right)_T \mathrm{d}p \tag{2}$$

and using the following thermodynamic relations,

$$\left(\frac{\partial s}{\partial T}\right)_p = \frac{1}{T}\left(\frac{\partial h}{\partial T}\right)_p,\ \left(\frac{\partial s}{\partial p}\right)_T = -\left(\frac{\partial v}{\partial T}\right)_p \tag{3}$$

the differential change in entropy for any pure fluid can be expressed in a general form [12, 13]:

$$\mathrm{d}s = \frac{c_p}{T}\mathrm{d}T - \beta_v v\,\mathrm{d}p \tag{4}$$

where β_v is the thermal expansion coefficient. Using Equations (4) and (1) and integrating from the inlet to the exit, the total generation of entropy in the heat exchanger is obtained. We can identify a thermal component, associated with irreversible heat transfer along a finite temperature difference, and a pressure component, associated with the pressure loss due to viscous flow:

$$\dot{S}_{irr} = \int_i^e \mathrm{d}\dot{S}_{irr} = \dot{S}_{irr,\Delta T} + \dot{S}_{irr,\Delta p} \tag{5}$$

where,

$$\begin{aligned}
\dot{S}_{irr,\Delta T} &= \dot{m}_A \left(\int_{T_i}^{T_e} \frac{c_p}{T}\mathrm{d}T\right)_A + \dot{m}_B \left(\int_{T_i}^{T_e} \frac{c_p}{T}\mathrm{d}T\right)_B \\
\dot{S}_{irr,\Delta p} &= -\dot{m}_A \left(\int_{p_i}^{p_e} \beta_v v\,\mathrm{d}p\right)_A - \dot{m}_B \left(\int_{p_i}^{p_e} \beta_v v\,\mathrm{d}p\right)_B
\end{aligned} \tag{6}$$

The rate of irreversible entropy generation is important in exergetic analysis because it is proportional to the rate of exergy destruction:

$$\dot{B}_{irr} = T_0 \cdot \dot{S}_{irr} \tag{7}$$

In TMS applications, we have to consider the amount of exergy that was successfully transferred (or otherwise lost) during charge in order to determine the maximum work that can be recovered during discharge. This process is illustrated in Figure 1, where exergy, in the form of thermal availability, is being transferred to a fluid storage medium by means of a heat exchanger. $\Delta\dot{B}_A$ and $\Delta\dot{B}_B$ express the rate of exergy change of each stream. They have opposite signs and, in the absence of heat transfer to the environment, the sum of the two rates is equal to the rate of exergy loss. For either A or B:

$$\Delta\dot{B} = \dot{m}\Delta b = \dot{m}\,\Delta(h - T_0 s) = \dot{m}\left(\int_{h_i}^{h_e} \mathrm{d}h - T_0 \int_{s_i}^{s_e} \mathrm{d}s\right) \tag{8}$$

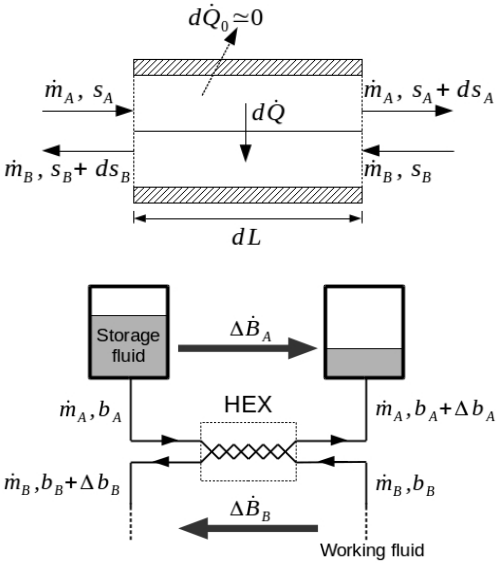

Figure 1: Above: Differential section of a heat exchanger. Below: Exergy transfer between the working fluid and the storage fluid using a heat exchanger.

By separating dh and ds in their temperature and pressure partial derivatives, we can identify again a thermal component and a pressure component, $\Delta\dot{B} = \Delta\dot{B}_{\Delta T} + \Delta\dot{B}_{\Delta p}$. After applying the relations in (3) once more,

$$\begin{aligned} \Delta\dot{B}_{\Delta T} &= \dot{m}\left(\int_{T_i}^{T_e} c_p \mathrm{d}T - T_0 \int_{T_i}^{T_e} \frac{c_p}{T}\mathrm{d}T\right) \\ \Delta\dot{B}_{\Delta p} &= \dot{m}\left(\int_{p_i}^{p_e} v\,(1-\beta_v T)\,\mathrm{d}p + T_0 \int_{p_i}^{p_e} \beta_v v\,\mathrm{d}p\right) \end{aligned} \tag{9}$$

We note that exergy is only transferred in the thermal form, $\Delta\dot{B}_{\Delta T}$, while $\Delta\dot{B}_{\Delta p}$ represents exergy destruction due to pressure loss within the HEX. A meaningful non-dimensional loss parameter is obtained by rationalising the rate of exergy loss by the rate of exergy transfer, as follows:

$$\xi \equiv \frac{T_0 \cdot \dot{S}_{irr}}{\left(-\Delta\dot{B}_{\Delta T,tm}\right)} \tag{10}$$

where the tm subscript refers to the exergy transfer medium and represents either A or B, depending on the case. Note that the transfer medium is the medium with highest initial exergy (the exergy *donor*), i.e. the hot stream when the HEX operates above T_0, and the cold stream when the HEX operates below T_0. The thermal and pressure components of the non-dimensional loss, $\xi_{\Delta T}$ and $\xi_{\Delta p}$, are simply found by separating $\dot{S}_{irr}$ in its two components, as in Equation (6).

Other common definitions of loss parameter may be found which rationalise the rate of exergy loss by the (absolute) exergy flow rate at the inlets of the HEX or by the heat capacity rate of one of the fluids, $\dot{m}c_p$. However, we prefer to avoid such definitions because they seem to imply that the loss tends to zero when the effectiveness of the HEX tends to zero, which is actually a highly irreversible situation. The definition we use seems particularly meaningful for TMS applications, since rate of exergy transfer is equivalent to (electrical) power input.

In the following sections, we will focus our interest on $\xi_{\Delta T}$ and on the impact that the variation of the specific heat capacity has on it.

2.2 The linear heat capacity model. Determination of temperature profiles and exergy loss

Real fluids are characterized by thermophysical properties that are a function of both temperature and pressure. While the temperature dependence may be strong, the pressure dependence is often weak and the pressure variation within a well-designed HEX will be small, allowing the analysis to concentrate on the effects of the temperature dependence. Particularly important for heat exchangers is the variation of the specific heat capacity, c_p. While monatomic gases are well modelled by the perfect gas approximation in which c_p is constant, the same is not generally true for diatomic and polyatomic gases and most liquids. Real fluids sometimes present a very complex temperature dependence, but a linear variation is often a good approximation within limited temperature ranges, allowing an analytical approach. Thus, we write:

$$c_p = \alpha\,(1+\sigma T) \tag{11}$$

where α is the constant component of c_p and σ is the coefficient determining its linear variation (a big σ implying a strong c_p variation per degree of temperature). Note that σ is positive in most cases, but can also be negative, particularly for gases close to the saturation curve and supercritical fluids. Typical values of σ range from $10^{-5}\mathrm{K}^{-1}$ to $10^{-3}\mathrm{K}^{-1}$ in magnitude.

If the two fluids operating in a HEX are different, their σ values will in principle be different and a pinch point will appear when trying to balance the two heat capacity rates, $\dot{m}c_p$. This is illustrated in Figures 2b and 2c, depending on whether the cold or the hot stream exhibits c_p variation. The pinch point (i.e. the point where the temperature difference between the streams is minimum) appears at a temperature T_p (defined on the cold stream), and, at that point, the temperature difference is ΔT_p. The corresponding distribution of temperature differences are plotted in Figure 3. In the case of a very large heat exchanger ($NTU \to \infty$), we would have $\Delta T_p \to 0$. Nevertheless, the temperature difference far from the pinch point would not collapse to zero, and irreversible heat transfer would continue to occur.

In the rest of the current section we will answer the following question: given known inlet temperatures (T_{c1} and T_{h2}), mass flow rates ($\dot{m}_c$ and $\dot{m}_h$) and a specified ΔT_p, how can we determine the temperature profiles of the HEX and the associated exergetic loss? The first task is to determine the pinch point temperature, T_p. Once this has been done, the total heat transfer rate and the corresponding outlet temperatures can be found, as will be shown.

With reference to Figures 2b and 2c, we can see that, depending on the case, the pinch point appears either somewhere in the middle of the HEX or at points 1 (left end) or 2 (right end). If it happens in the middle, then ΔT has a local minimum at that point. Since $\Delta T(\dot{Q}) = T_h(\dot{Q}) - T_c(\dot{Q})$, this implies,

$$\frac{\mathrm{d}\left(\Delta T(\dot{Q})\right)}{\mathrm{d}\dot{Q}} = 0 \Rightarrow \frac{\mathrm{d}T_h(\dot{Q})}{\mathrm{d}\dot{Q}} = \frac{\mathrm{d}T_c(\dot{Q})}{\mathrm{d}\dot{Q}} \tag{12}$$

To make further progress, we use the steady-flow energy equation in differential form. Neglecting changes in kinetic and potential energy within each stream:

$$\mathrm{d}\dot{Q} = \dot{m}\,\mathrm{d}h = \dot{m}\left(\left(\frac{\partial h}{\partial T}\right)_p \mathrm{d}T + \left(\frac{\partial h}{\partial p}\right)_T \mathrm{d}p\right) \simeq \dot{m}c_p\,\mathrm{d}T \tag{13}$$

where the latter is exact for perfect and semi-perfect gases, and a good approximation for any fluid as long as the pressure loss within the HEX is small. The condition from equation (12),

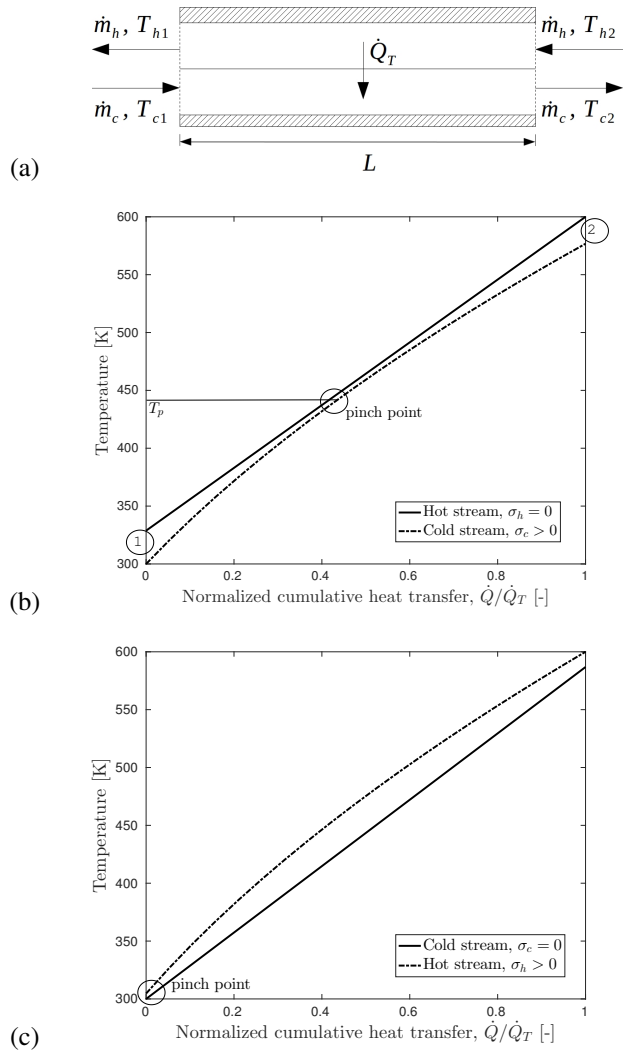

Figure 2: (a) Nomenclature of temperature inlets and outlets. (b) Generation of a pinch point due to c_p increase of the cold stream. (c) The same with c_p increase of the hot stream.

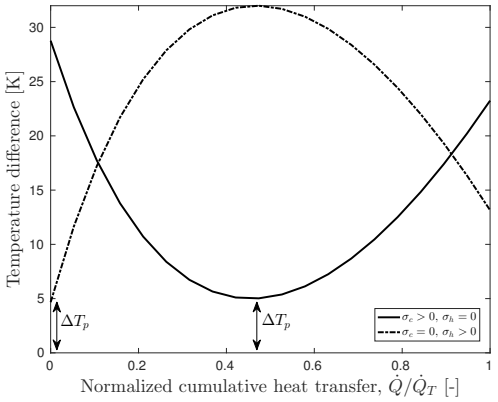

Figure 3: Temperature difference for the profiles presented in Figures 2b and 2c.

combined with Equation (13), means that the local heat capacity rate of both streams must be equal at the pinch point:

$$\dot{m}_h \cdot c_{p,h}(T_{p,h}) = \dot{m}_c \cdot c_{p,c}(T_{p,c}) \tag{14}$$

Using Equation (11),

$$\dot{m}_h \alpha_h \left(1 + \sigma_h \left(T_p + \Delta T_p\right)\right) = \dot{m}_c \alpha_c \left(1 + \sigma_c T_p\right) \tag{15}$$

After rearranging,

$$T_p = \frac{m_r \alpha_r \left(1 + \sigma_h \Delta T_p\right) - 1}{\sigma_c - \sigma_h m_r \alpha_r} \tag{16}$$

where $\alpha_r \equiv \alpha_h/\alpha_c$ and $m_r \equiv \dot{m}_h/\dot{m}_c$. However, the condition of equal local heat capacity rate could also represent a maximum of $\Delta T\left(\dot{Q}\right)$, in which case Equation (16) would not be valid and the pinch point would occur at either 1 or 2, instead. A general and systematic way to find out in which of the three possible positions the pinch point actually occurs is presented below.

Suppose that the pinch point occurs at 1. In this case, we know that $T_{h1} = T_{c1} + \Delta T_p$, and the total heat transfer rate can be calculated by computing the rate in enthalpy change of the hot stream (which is a function of T_{h1} and T_{h2}). Using Equations (13) and (11),

$$\dot{Q}_{T,1} = \int_0^{\dot{Q}_T} \mathrm{d}\dot{Q}_h = \dot{m}_h \int_{T_{c1}+\Delta T_p}^{T_{h2}} c_{p,h}\,\mathrm{d}T_h \tag{17}$$

Similarly, if the pinch point occurs at 2, we know that $T_{c2} = T_{h2} - \Delta T_p$, and then we can calculate it by computing the rate in enthalpy increase of the cold stream,

$$\dot{Q}_{T,2} = \int_0^{\dot{Q}_T} \mathrm{d}\dot{Q}_c = \dot{m}_c \int_{T_{c1}}^{T_{h2}-\Delta T_p} c_{p,c}\,\mathrm{d}T_c \tag{18}$$

Finally, if it happens in the middle, then,

$$\dot{Q}_{T,p} = \dot{m}_c \int_{T_{c1}}^{T_p} c_{p,c}\mathrm{d}T_c + \dot{m}_h \int_{T_p+\Delta T_p}^{T_{h2}} c_{p,h}\,\mathrm{d}T_h \tag{19}$$

where T_p is obtained from Equation (16). In the case of linear c_p variation, the analytical solutions of Equations (17), (18) and (19) are obtained by straightforward integration using the $c_p(T)$ expression given by Eq. (11). It can be shown that the actual value of the total heat transfer rate must be the minimum of the three integrals, which in turn indicates the actual pinch point location, i.e.

$$\dot{Q}_T = \min\left(\dot{Q}_{T,1}, \dot{Q}_{T,2}, \dot{Q}_{T,p}\right) \tag{20}$$

To better understand this statement, consider Figure 4, where an example scenario with $\sigma_h > 0$, $\sigma_c < 0$ and $\Delta T_p = 30\,\mathrm{K}$ is presented. The two continuous lines correspond the actual thermal profiles of the two streams. The pinch point appears at

1, and the total heat transfer rate can be computed by Eq. (17), i.e. $\dot{Q}_T = \dot{Q}_{T,1}$. Important to realize is that the values predicted by $\dot{Q}_{T,2}$ and $\dot{Q}_{T,p}$ (which are incorrect) will necessarily be bigger than the one obtained from $\dot{Q}_{T,1}$. This is because $T_{c1} = 300\,\mathrm{K}$ and $T_{h2} = 600\,\mathrm{K}$ are fixed values, and in order to produce the temperature difference of 30 K elsewhere in the HEX, the two temperature curves would have to become closer to each other, meaning that the heat transfer rate would have to be higher. For instance, in order to compute $\dot{Q}_{T,p}$, we first apply Eq. (16), which in this case (incorrectly) predicts $T_p = 457\,\mathrm{K}$ (corresponding to a local maximum in ΔT instead of a local minimum). The only way to produce a temperature difference equal to 30 K at the new predicted T_p is to increase the rate in enthalpy change of both streams, bringing them closer together, as shown by the dotted lines in the same graph. In this example, the solution provided by $\dot{Q}_{T,p}$ is not only incorrect but it also provides a physically impossible result, where the two temperature profiles cross themselves and $T_{h1} < T_{c1}$. Something similar, although less extreme, happens when using the solution provided by $\dot{Q}_{T,2}$.

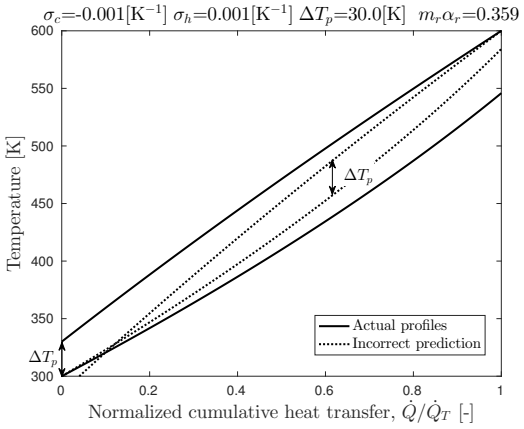

Figure 4: Actual temperature profiles (continuous lines, predicted by $\dot{Q}_{T,1}$) and incorrect temperature profiles (dotted lines, predicted by $\dot{Q}_{T,p}$). In the second case, the two curves are closer to each other because $\dot{Q}_{T,p} > \dot{Q}_{T,1}$.

The actual value of the total heat transfer rate is therefore found by separately computing the integrals in Equations (17), (18) and (19) and selecting the minimum of the three, as stated by Eq. (20).

Once the actual $\dot{Q}_T$ is known, an analytical expression of the temperature distributions can be found. In the case of the hot stream, this is done by changing the lower limits of integration in Equation (17) by $\dot{Q}$ (instead of 0) and $T_h\left(\dot{Q}\right)$ (instead of T_{h1}), and then rearranging:

$$T_h(\dot{Q}) = \pm\sqrt{\left(T_{h2} + \frac{1}{\sigma_h}\right)^2 - \frac{2\left(\dot{Q}_T - \dot{Q}\right)}{\sigma_h \dot{m}_h \alpha_h}} - \frac{1}{\sigma_h} \quad ; \quad \sigma_h \neq 0$$

or

$$T_h(\dot{Q}) = T_{h2} - \frac{\dot{Q}_T - \dot{Q}}{\dot{m}_h \alpha_h} \quad ; \quad \sigma_h = 0 \tag{21}$$

Similarly, in the case of the cold stream, Equation (18) is adapted by changing the upper limits of integration by $\dot{Q}$ (instead of $\dot{Q}_T$) and $T_c\left(\dot{Q}\right)$ (instead of T_{c2}). After rearranging:

$$T_c(\dot{Q}) = \pm\sqrt{\left(T_{c1} + \frac{1}{\sigma_c}\right)^2 + \frac{2\dot{Q}}{\sigma_c \dot{m}_c \alpha_c}} - \frac{1}{\sigma_c} \quad ; \quad \sigma_c \neq 0$$

or

$$T_c(\dot{Q}) = T_{c1} + \frac{\dot{Q}}{\dot{m}_c \alpha_c} \quad ; \quad \sigma_c = 0 \tag{22}$$

In Equations (21) and (22), the $\pm$ sign in front of the square roots is taken positive for $\sigma > 0$ and negative for $\sigma < 0$. The unknown temperature ends are found by noting that $T_{c2} = T_c(\dot{Q}_T)$ and $T_{h1} = T_h(0)$. Furthermore, since $\dot{Q}$ and $\dot{Q}_T$ are always divided by $\dot{m}_h\alpha_h$ or $\dot{m}_c\alpha_c$ in the above expressions, we note that the temperature distributions (and the outlet temperatures) become a function of the product of ratios $m_r\alpha_r$ and independent of the actual values of each $\dot{m}$ and α. The problem is therefore reduced to six independent variables: T_{c1}, T_{h2}, $m_r\alpha_r$, σ_h, σ_c and ΔT_p. Once the exit temperatures have been found, evaluating the thermal component of the entropy generation rate, $\dot{S}_{irr,\Delta T}$, and the corresponding non-dimensional exergy loss, $\xi_{\Delta T}$, is done by straightforward integration of the Equations (6) and (9) and substitution in (10). Therefore, $\xi_{\Delta T}$ is a function of the six independent parameters just mentioned plus the ambient temperature, T_0.

2.3 Test cases

2.3.1 c_p variation on one stream

Before applying the above analysis to a test case, it is worth mentioning that all results presented in this section have been generated using the analytical expressions introduced so far, and have been checked against numerical solutions which yield identical values.

In a first test case, the fluid circulating in the hot stream of the HEX is chosen to have constant c_p ($\sigma_h = 0$), while the cold one increases with temperature ($\sigma_c > 0$), as in Figure 2b. Note again that in the current analysis ΔT_p is taken as a fixed design parameter (which ultimately depends on the geometry and operating conditions of the HEX). T_p, on the other hand, is allowed to change when varying the ratio of the mass flow rates, m_r, according to Equation (16). Considering this, the outlet temperatures and the corresponding thermal exergy loss are computed following the procedure explained in section 2.2, for three different values of ΔT_p and a range of m_r values.

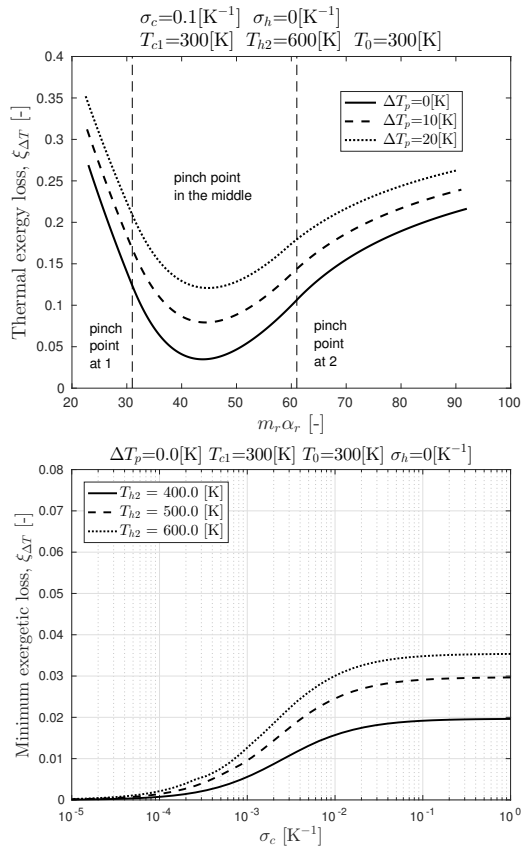

Figure 5: Thermal exergetic loss for $\sigma_h = 0$ and $\sigma_c > 0$.

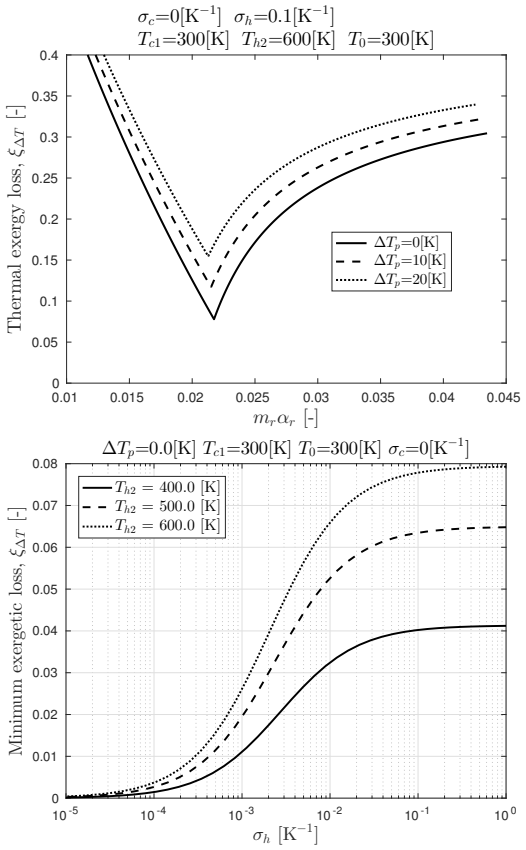

Figure 6: Thermal exergetic loss for $\sigma_c = 0$ and $\sigma_h > 0$.

The results of the loss analysis are presented in Figure 5. The top graph, made for the case of $\sigma_c = 0.1\,\mathrm{K}^{-1}$, shows the variation of $\xi_{\Delta T}$ as a function of $m_r\alpha_r$, with a minimum of $\xi_{\Delta T} = 3.5\,\%$ (for $\Delta T_p = 0\,\mathrm{K}$) at $m_r\alpha_r \simeq 43.9$. The two vertical lines show the instances at which the pinch point reaches T_{c1} and T_{h2}. The strong variation of the loss indicates the importance of optimising the m_r value (α_r is fixed, given by the fluids properties), particularly for low ΔT_p values.

The bottom graph in Figure 5 shows the evolution of the minimum $\xi_{\Delta T}$ (i.e for the corresponding optimised $m_r\alpha_r$ value) as a function of σ_c, ranging from $\sigma_c \ll 1/T_{c1}$ (constant c_p) to $\sigma_c \gg 1/T_{c1}$ (c_p dominated by its linear component). The plot presents the loss for the case with $\Delta T_p = 0$ and three different values of T_{h2}, showing that the loss is bigger when the ratio $T_{h2}/T_{c1} \equiv \phi$ increases. This is consequence of the fact that, for a fixed σ_c, the total variation of c_p experienced by the cold stream increases when ϕ increases. Further results also show that the loss due to a given finite $\Delta T_p > 0$ decreases with ϕ, meaning that the impact of c_p variation can become dominant as ϕ increases, even if it is negligible for cases with small ϕ.

A similar study has also been performed for the case of constant $c_{p,c}$ ($\sigma_c = 0$) and linear $c_{p,h}$ ($\sigma_h > 0$), as in Figure 2c. Now the pinch point can only occur at one of the two temperature ends, or at both ends simultaneously, but never in between. The optimal $m_r\alpha_r$ value, in exergetic terms, is found to be the one that makes the pinch point occur at both ends, for which the exergetic loss presents a sharp minimum, as shown in the top graph in Figure 6. It is possible to find an analytical expression of this optimal $m_r\alpha_r$ value by imposing that the total heat transfer rate as calculated by Equations (17) and (18) must be the same, giving:

$$(m_r\alpha_r)_{optimal} = \frac{T_{h2} - T_{c1} - \Delta T_p + \dfrac{\sigma_c}{2}\left((T_{h2} - \Delta T_p)^2 - T_{c1}^2\right)}{T_{h2} - T_{c1} - \Delta T_p + \dfrac{\sigma_h}{2}\left(T_{h2}^2 - (T_{c1} + \Delta T_p)^2\right)} \tag{23}$$

This expression is found to be exact for situations with $\sigma_h > \sigma_c$. For the opposite situations, when $\sigma_h < \sigma_c$, the expression is not exact but still accurate, particularly for small values of ΔT_p. This is important for energy storage applications because it means that optimising the mass flow ratio between the working fluid and the storage fluid during charge is consistent with minimizing the exergetic loss also during discharge (since the same mass flow ratio must be used during charge and discharge to completely consume the energy stored during charge).

The minimum exergetic loss as a function of σ_h is shown in the bottom graph in Figure 6. We observe a similar behaviour to that described in the previous case (see Figure 5), with the difference that the absolute value of the loss is about twice as big. This can be understood by comparing the T-Q diagrams of Figures 2b and 2c, where one can see that the area enclosed by

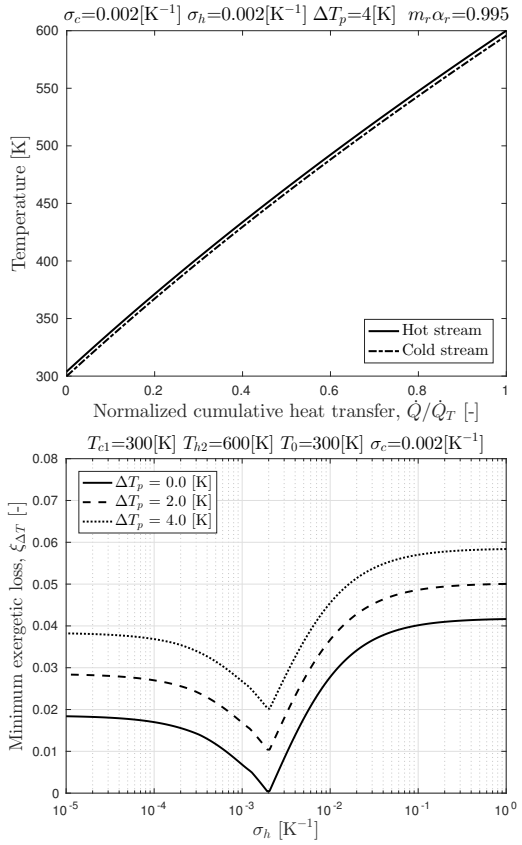

Figure 7: Above: Temperature profiles for $\sigma_h = \sigma_c$ and optimal m_r. Below: Minimum exergetic loss for $\sigma_c = 2 \cdot 10^{-3}\,\mathrm{K}^{-1}$ and different σ_h values.

the two temperature curves, which drives the irreversible heat transfer, tends to be larger in the second case.

Similar phenomena are observed when studying cases where either σ_c or σ_h are negative.

2.3.2 c_p variation on both streams

Having studied the effects of c_p variation on the cold and on the hot streams separately, the study of specific combinations of both becomes straightforward. The following observations, however, should be noticed:

- For cases with $\sigma_c > \sigma_h$, the pinch point and loss behaviour are similar to the case with constant $c_{p,h}$ and increasing $c_{p,c}$.
- For cases with $\sigma_h > \sigma_c$, the pinch point and loss behaviour are similar to the case with constant $c_{p,c}$ and increasing $c_{p,h}$.
- For cases with $\sigma_{c,h} \neq 0$ but $\sigma_c = \sigma_h$, the two lines in the $T\left(\dot{Q}\right)$ diagram are curved but maintain a constant ΔT between each other when the optimised m_r value is used, as shown in the top graph of Figure 7. This scenario is quite similar to a situation with both fluids having constant c_p, and no pinch point appears when the heat capacity rates are balanced. In the bottom of the same Figure, the minimized exergetic loss (for optimal m_r) has been plotted as a function of σ_h for three ΔT_p values, given a fixed $\sigma_c = 2 \cdot 10^{-3}\,\mathrm{K}^{-1}$. Noticeably, the optimised $\xi_{\Delta T}$ presents a sharp minimum when σ_h is also $2 \cdot 10^{-3}\,\mathrm{K}^{-1}$.

3 Numerical study

3.1 Determination of the required heat transfer area

In the previous sections, we have focused our attention on the determination of the temperature profiles, and their associated exergy loss given known operating conditions and assuming a specified value of ΔT_p. In actual heat exchangers, this last parameter will be determined by the geometry (which affects the total heat transfer coefficient, U_T) and by the total heat transfer area, A_T. In this section, we consider how to find the required $U_T A_T$ to satisfy a specified ΔT_p, using the linear c_p model.

By definition of the total heat transfer coefficient,

$$\mathrm{d}\dot{Q} = U_T \Delta T \mathrm{d}A \tag{24}$$

where all the parameters correspond to an infinitesimal section of the HEX. Integrating from the cold end until a given section,

$$\int_0^{A(\dot{Q})} U_T \mathrm{d}A = \int_0^{\dot{Q}} \frac{\mathrm{d}\dot{Q}}{\Delta T\left(\dot{Q}\right)} \tag{25}$$

While, in general, U_T will vary at different sections of the HEX, a satisfactory approximation is normally obtained by considering its average value, so that the left hand side of the previous equation becomes $\simeq \bar{U}_T A\left(\dot{Q}\right)$. To solve the right hand side of the same equation, we need the expression for $\Delta T\left(\dot{Q}\right)$, which is obtained by subtracting Eq. (22) from (21),

$$\begin{aligned} \Delta T\left(\dot{Q}\right) \;=\; & \sqrt{\left(T_{h2} + \frac{1}{\sigma_h}\right)^2 - \frac{2\left(\dot{Q}_T - \dot{Q}\right)}{\sigma_h \dot{m}_h \alpha_h}} - \frac{1}{\sigma_h} \\ & - \sqrt{\left(T_{c1} + \frac{1}{\sigma_c}\right)^2 + \frac{2\dot{Q}}{\sigma_c \dot{m}_c \alpha_c}} + \frac{1}{\sigma_c} \end{aligned} \tag{26}$$

Unfortunately, the right-hand-side integral in Eq. (25) does not have an exact analytical solution for such a form of $\Delta T\left(\dot{Q}\right)$. An approximation of $\Delta T\left(\dot{Q}\right)$ can be obtained by using a Taylor expansion of Eq. (26) around $\dot{Q} = \dot{Q}_T/2$ up to the second order, therefore writing $\Delta T\left(\dot{Q}\right) \approx a\dot{Q}^2 + b\dot{Q} + c$. Such alternative expression can be integrated, providing a closed-form analytical solution which is a good approximation in most common circumstances. On the other hand, numerical integration provides an even more accurate value and can be used for any form of $c_p(T)$, and is therefore recommended. In the following, $\bar{U}_T A_T$ is obtained by numerically integrating Eq. (25) from 0 to $\dot{Q}_T$. Then, the product can be non-dimensionalised to become the

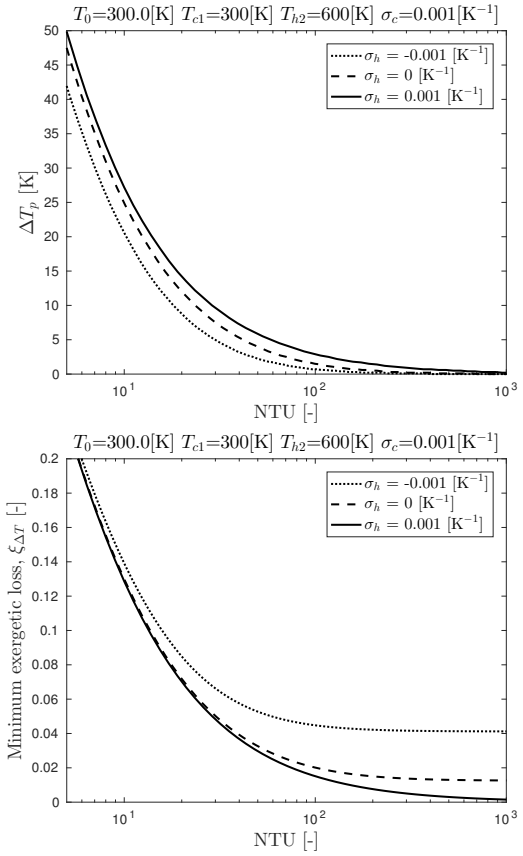

Figure 8: Temperature difference at the pinch point, and minimum exergetic loss for a given Number of Transfer Units and optimised $m_r\alpha_r$.

Number of Transfer Units on an averaged form:

$$\text{NTU} \equiv \frac{\bar{U}_T A_T}{\min\left(\dot{m}_h \bar{c}_{p,h}, \dot{m}_c \bar{c}_{p,c}\right)} \tag{27}$$

The NTU is an important parameter in HEX design and it is the basis of the effectiveness-NTU method [14]. While the method is only valid for situations where c_p variation is negligible, computing the NTU still provides a valuable reference in terms of HEX size.

The top graph in Figure 8 presents the variation of ΔT_p with NTU for three different σ_h values and a fixed σ_c value. In all three scenarios $m_r\alpha_r$ was optimised. Noticeably, the two curves with $\sigma_h < \sigma_c$ fall towards $\Delta T_p = 0$ faster than the curve with $\sigma_h = \sigma_c$, indicating the presence of a pinch point –and faster heat transfer due to higher ΔT everywhere else. In the third case, ΔT is constant everywhere and decreases slower. The bottom graph plots $\xi_{\Delta T}$ for the same three cases. For small NTU, the three curves converge, meaning that c_p variation is not an issue for low-performance HEXs. For high NTU (i.e. high-performance), however, the pinch point created in the first two cases (dotted and dashed lines) gives rise to a minimum $\xi_{\Delta T}$, while in the third scenario (solid line) no pinch point appears and $\xi_{\Delta T}$ steadily decreases with NTU. Finally, the generation of such plots allows the determination of the necessary NTU to obtain a given ΔT_p or a given $\xi_{\Delta T}$. Once the NTU is known, the total heat transfer area of the HEX is obtained from Eq. (27).

3.2 Minimum exergetic loss for real fluids

Along sections 2.2 and 2.3, the assumption of a linear dependence of c_p with temperature has permitted a better understanding of the generation and behaviour of pinch points in the HEX and of the loss associated with them. While in several cases this approximation is satisfactory, in others it fails to properly describe the variation, therefore predicting incorrect values of the outlet temperatures and of the exergy loss. In such cases, a numerical method becomes necessary. The method implemented here follows similar steps as the ones described in the analytical study but using numerical integration and including the actual $c_p(T)$ functions instead of the linear model:

1. An initial mass flow ratio m_r is selected (for example, such that the estimated average heat capacity rates match) and a given ΔT_p is chosen (zero if the minimum loss is to be found).

2. The condition from Equation (14) is used to find the temperature of the expected pinch point (which might or might not correspond to the actual pinch point). The total heat transfer rate, $\dot{Q}_T$, then is found by selecting the minimum of the values obtained by the three integrals in Equations (17), (18) and (19). That also determines the actual pinch point location.

3. Once $\dot{Q}_T$ is known, the outlet temperatures are found by knowledge of the inlet temperatures and numerically integrating the differential Equation (13).

4. The associated thermal exergy loss is computed via Equations (6), (9) and (10).

5. Finally, the process is repeated for a range of m_r values until the optimal m_r, corresponding to the minimum $\xi_{\Delta T}$, is found.

Table 1 presents the minimum exergetic loss corresponding to various combinations of fluids that are attractive for some TMS systems. The selected fluids and their temperature and pressure conditions are based on the conditions proposed in the literature. In the case of the CHEST system (a PTES system based on the Rankine cycle), the top temperature proposed in [4] does not exceed 400°C, but here it was set to 550°C to know what the minimum loss would be if the whole operability range of the liquid Solar Salt was exploited (therefore maximizing its energy density). In the case of the CAES systems, temperature and pressure conditions vary considerably from one system to another and can also vary from one stage to another in multi-stage systems. Therefore, the selected scenarios for CAES might not be representative of other systems. The JB-PTES systems in the table refer to the Joule-Brayton (gas cycle) version of PTES. The usage of Solar Salt and ethanol as storage liquids (among others), in substitution of the solid thermal reservoirs, was proposed on an

Potential applications	**Storage fluid working fluid**	**Pressure** [bar]	$\mathbf{T_{c1}}$ / $\mathbf{T_{h2}}$ [°C]	σ [$10^{-4}\,K^{-1}$]	$\mathbf{R^2}$ [-]	$\xi_{\Delta T}$ (analytic) [%]	$\xi_{\Delta T}$ (numeric) [%]
CAES [15]	Water	2	25 / 120	1.6	0.89	1.80	1.80
	Air	100		-5.5	0.97		
CHEST [4]	Solar Salt	1	312 / 550	1.2	-	2.55	2.51
	Steam	100		-10.1	0.69		
JB-PTES and CAES [8]	Solar Salt	1	200 / 550	1.2	-	0.12	0.11
	Air	50		1.9	0.99		
JB-PTES	Ethanol	1	-103 / 25	36.1	0.95	7.51	7.05
	Argon	1		-0.5	0.93		
JB-PTES	Oxygen	1	-218 / -183	3.7	0.86	0.11	0.09
	Helium	1		-0.2	0.96		
JB-PTES [16]	Isopentane	1	-153 / 25	25.9	0.95	4.83	3.90
	Hydrogen	20		10.7	0.94		
TEES [6]	Water	2	25 / 120	1.6	0.89	6.18	8.89
	Carbon Dioxide	160		-14.2	0.21		

Table 1: Comparison of the minimum loss $\xi_{\Delta T}$ obtained with the analytical linear c_p approximation and with the numerical method. In this table, $\xi_{\Delta T}$ represents the combined loss for the charge and discharge processes.

internal report at CUED [17]. This cycle is a current focus of research, as a result of which a combination of liquid oxygen (storage medium) and helium (working fluid) is also being proposed [18]. The combination of liquid isopentane (storage medium) and hydrogen (working fluid) was proposed by the authors of [16].

In Table 1, both the analytical and the numerical methods are used to predict the minimum exergetic loss. The loss is computed twice, taking first one fluid as the hot stream and the other as the cold stream, and vice-versa, and added up (corresponding to a charge and discharge scenario). The $c_p(T)$ functions (at the given constant pressure) were obtained using the CoolProp library [19], except for the Solar Salt, obtained from [20]. The σ value used in the analytical method is found by applying a linear regression curve, and the quality of the fit is evaluated with the coefficient of determination R^2.

While in some fluid couples the effect of c_p variation is irrelevant (e.g. Solar Salt and Air), in others the minimum exergy loss is clearly non-negligible (e.g. Ethanol and Argon). A satisfactory agreement between the analytical and the numerical method is found in most cases. In the case of the HEX operating with liquid H_2O and supercritical CO_2, however, the linear fit is very poor due to the complex dependence of the CO_2's heat capacity, and the loss is underestimated by 30 %. Figure 9 shows the (mean-normalized) c_p variation of H_2O and CO_2, and the pinch point generated for $\Delta T_p = 0$. The case is based on the PTES system proposed in [6], where liquid water is used as storage media and supercritical CO_2 as working fluid. The authors of that article also propose a stream splitting mechanism which allows to change the heat capacity rate of the water by increasing or decreasing its mass flow rate at different temperature levels, therefore adapting to the heat capacity curve of the CO_2. While a perfect adaptation would require an infinite

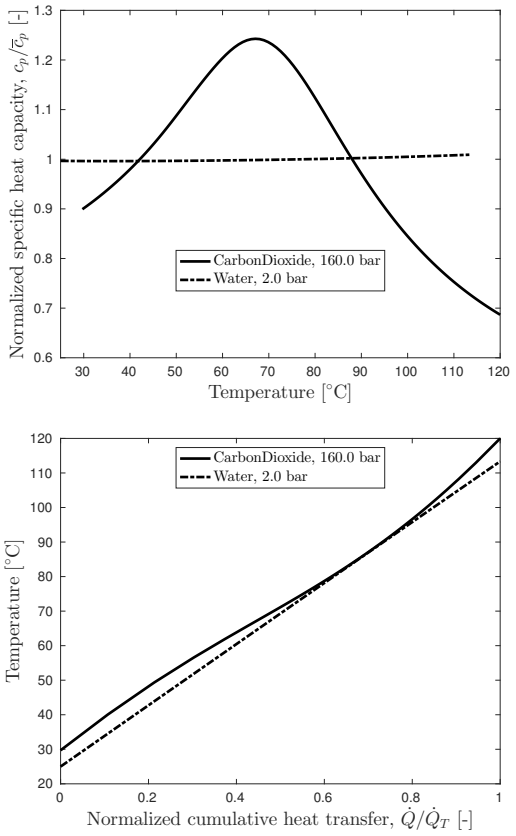

Figure 9: c_p variation and pinch point generation on a HEX operating with water and supercritical CO_2.

number of splits (i.e. infinite number of sections with different levels of water mass flow rate), a finite number of splits (e.g. 4-6) is enough to considerably reduce the exergetic loss. In practice, each section constitutes a separate HEX within a Heat Exchanger Network (HEN) (or a section within an equivalent multi-stream HEX), and for each new section a new water tank is necessary to store/deliver water at the adequate temperature. A graphical procedure to determine the temperature levels and storage capacities of each tank is presented in [21]. While such mechanism effectively enables the usage of fluids with strong c_p variation without implying a high exergy loss, the additional costs of the tanks and the HEN and the increased complexity in terms of design and operation has to be accounted for.

3.3 Effect on the optimisation of a flat-plate heat exchanger

Heat capacity variation does not only set a minimum exergetic loss but also affects the optimal design of the HEX. In order to show this, a one-dimensional, steady-state model of a counter-flow HEX was developed, which iteratively solves the energy equation between the two flow streams until the temperature profiles converge. The model used in this work was developed independently, but a detailed description of a similar scheme may be found in [22]. Heat transfer coefficients and friction factors are computed using standard correlations for a flat-plate geometry [23], and pressure losses due to flow friction in the HEX core are computed accordingly [10]. Therefore, the code is able to determine the two exergy loss parameters, $\xi_{\Delta T}$ and $\xi_{\Delta p}$, thus allowing the adaptation of the design characteristics until an optimal point is found.

By setting constant thermophysical properties, it was possible to reproduce the results described in [23]. These show that there are two internal geometric characteristics that can be optimised for a given external geometry: the ratio between the plate separation allowed for each stream (which regulates the balance of pressure losses between the two streams), and the total heat transfer area (which regulates the balance between heat transfer and pressure losses). After validating the model using constant properties, real properties were introduced using the CoolProp library, and it was observed that the generated temperature profiles also compared satisfactorily with those obtained with the analytical and numerical methods presented in the previous sections of this article.

Finally, it was found that c_p variation can considerably affect the selection of optimal design parameters such as the total heat transfer area. This is shown in Figure 10, where the dimensionless exergy loss of a HEX operating with argon (hot stream) and ethanol (cold stream) is plotted once using constant (averaged) properties and once using real properties. The thermal component, $\xi_{\Delta T}$, and the total loss, $\xi = \xi_{\Delta T} + \xi_{\Delta p}$, are plotted separately. It is seen that, while in the first case $\xi_{\Delta T}$ continuously decreases with increasing surface, in the second case the generation of a pinch point due to the ethanol's strong c_p variation creates a plateau on the value of $\xi_{\Delta T}$, which increases the total loss and decreases the value of the optimal heat transfer area. Noting the logarithmic scales used in the graph, the minimum loss is 5 times bigger and the optimal area 30 % smaller. Furthermore, it is important to note that this effect has not only thermodynamic but also economic implications, since the total heat transfer area is directly proportional to the amount of material needed to build the HEX (for a given plate thickness), and therefore sets a lower limit to the total cost of the component.

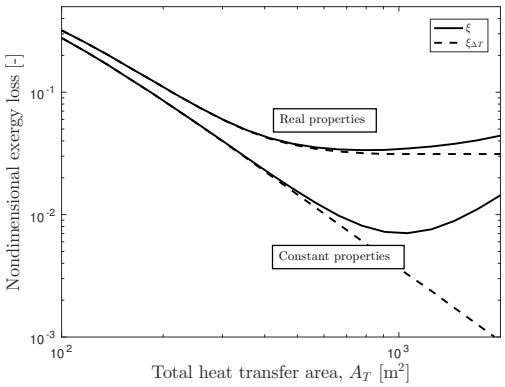

Figure 10: Effect of the pinch point generation on the optimal heat transfer area.

4 Conclusions

The temperature dependence of the specific heat capacity of some real fluids generates pinch points that force irreversible heat transfer and set a minimum exergetic loss on heat exchangers.

An analytical study of this phenomenon has been presented assuming linear heat capacity variation, which is useful in understanding both the nature and the extent of the problem. The analytical study reveals and validates interesting trends, such as:

- The value of the minimum exergetic loss obtained for a given combination of two fluids varies considerably depending on what fluid operates as the hot stream and what fluid operates as the cold stream. Moreover, the loss increases when the distance between the two temperature ends, T_{c1} and T_{h2}, increases.
- Heat capacity variation is not a problem in itself, but difference in variation is. The minimum exergetic loss obtained by two fluids that present exactly the same $c_p(T)$ function is zero.
- The exergetic loss is extremely sensitive to the ratio of mass flow rates, stressing the need to operate at the optimal value. Additionally, this optimal value is found to be similar for the charge and discharge operations.
- While the effect of heat capacity variation may be neglected in devices with a low number of transfer units, its

consideration becomes critical to accurately predict the efficiency of high-performance heat exchangers.

The linear approximation is found to be applicable to many real fluids within temperature ranges that are relevant for thermo-mechanical storage systems. For fluids that present more complex dependencies, a numerical method can be used instead.

Finally, a one-dimensional, steady-state model of a flat-plate, counter-flow heat exchanger is used to predict the temperature distributions and pressure losses corresponding to given operating conditions. The model accounts for real thermophysical properties and can be used to optimize the geometry and minimize the total exergy loss. Pinch points generated by heat capacity variation are found to have an impact on the optimal heat transfer area of the heat exchanger.

Acknowledgements

P. Farres-Antunez gratefully acknowledges Peterhouse for the graduate research studentship which is allowing him to perform this research project at Cambridge University Engineering Department.

Nomenclature

Symbols

Symbol	Description	Units
α	Constant component of c_p	$\mathrm{J\,kg^{-1}\,K^{-1}}$
α_r	Defined as: $\alpha_r \equiv \alpha_h/\alpha_c$	$-$
β_v	Thermal expansion coefficient, $\beta_v \equiv (1/v)\,(\partial v/\partial T)_p$	$\mathrm{K^{-1}}$
σ	Linear c_p coefficient	$\mathrm{K^{-1}}$
ϕ	Ratio between T_{h2} and T_{c1}	$-$
ξ	Non-dimensional exergy loss	$-$
A_T	Total heat transfer area	$\mathrm{m^2}$
$\dot{B}_{irr}$	Exergy destruction rate	W
$\Delta\dot{B}$	Rate of exergy change	W
c_p	Isobaric specific heat capacity	$\mathrm{J\,kg^{-1}\,K^{-1}}$
h	Specific enthalpy	$\mathrm{J\,kg^{-1}}$
L	Heat exchanger length	m
$\dot{m}$	Mass flow rate	$\mathrm{kg\,s^{-1}}$
m_r	Defined as: $m_r \equiv \dot{m}_h/\dot{m}_c$	$-$
p	Pressure	Pa
$\dot{Q}$	Cumulative heat transfer rate, $0 \leq \dot{Q} \leq \dot{Q}_T$	W
$\dot{Q}_p$	Cumulative heat transfer rate at pinch point	W
$\dot{Q}_T$	Total heat transfer rate	W
s	Specific entropy	$\mathrm{J\,kg^{-1}\,K^{-1}}$
$\dot{S}_{irr}$	Entropy generation rate	$\mathrm{W\,K^{-1}}$
T	Temperature	K
T_0	Ambient temperature	K
T_p	Temperature of the cold stream at the pinch point	K
ΔT	Temperature difference	K
ΔT_p	Temperature difference at pinch point	K
U_T	Total heat transfer coefficient	$\mathrm{W\,m^{-2}\,K^{-1}}$
v	Specific volume	$\mathrm{m^3\,kg^{-1}}$

Subscripts

1, 2	Heat exchanger ends; 1 is the cold stream inlet, 2 is hot stream inlet
A, B	Stream A, stream B
c, h	Cold stream, hot stream
i, e	Inlet, exit
tm	Transfer medium
ΔT, Δp	Temperature and pressure components

Acronyms

CAES	Compressed air energy storage
CHEST	Compressed heat energy storage
CUED	Cambridge University Engineering Department
HEX	Heat exchanger
HEN	Heat exchanger network
LAES	Liquid air energy storage
NTU	Number of transfer units
PTES	Pumped thermal energy storage
TMS	Thermo-mechanical energy storage

References

[1] D.J.C. MacKay. *Sustainable Energy - without the hot air*. UIT Cambridge, 2008. Available free online from www.withouthotair.com.

[2] A.J. White, G. Parks, and C. Markides. Thermodynamic analysis of pumped thermal electricity storage. *Applied Thermal Engineering*, 53(2):291–298, 2013.

[3] T. Desrues, J. Ruer, P. Marty, and J. F. Fourmigué. A thermal energy storage process for large scale electric applications. *Applied Thermal Engineering*, 30(5):425–432, 2010.

[4] W. D. Steinmann. The CHEST (Compressed Heat Energy STorage) concept for facility scale thermo mechanical energy storage. *Energy*, 69:543–552, 2014.

[5] Samuel Henchoz, Florian Buchter, Daniel Favrat, Matteo Morandin, and Mehmet Mercangöz. Thermoeconomic analysis of a solar enhanced energy storage concept based on thermodynamic cycles. *Energy*, 45(1):358–365, 2012.

[6] Mehmet Mercangöz, Jaroslav Hemrle, Lilian Kaufmann, Andreas Z'Graggen, and Christian Ohler. Electrothermal energy storage with transcritical CO2 cycles. *Energy*, 45(1):407–415, 2012.

[7] Robert Morgan, Stuart Nelmes, Emma Gibson, and Gareth Brett. Liquid air energy storage - Analysis and first results from a pilot scale demonstration plant. *Applied Energy*, 137:845–853, 2015.

[8] Chris Bullough, Christoph Gatzen, Christoph Jakiel, Martin Koller, Andreas Nowi, and Stefan Zunft. Advanced Adiabatic Compressed Air Energy Storage for the Integration of Wind Energy. *Proceedings of the European Wind Energy Conference*, (November):22–25, 2004.

[9] J.E Hesselgreaves. Rationalisation of second law analysis of heat exchangers. *International Journal of Heat and Mass Transfer*, 43(22):4189–4204, 2000.

[10] F.P. Incropera, D.P. DeWitt, T.L. Bergman, and A.S. Lavine. *Fundamentals of Heat and Mass Transfer*. John Wiley and Sons, 6th edition, 2007.

[11] M Yilmaz, O.N Sara, and S Karsli. Performance evaluation criteria for heat exchangers based on second law analysis. *Exergy, An International Journal*, 1(4):278–294, 2001.

[12] Giuseppe Grazzini and Fabio Gori. Entropy parameters for heat exchanger design. *International Journal of Heat and Mass Transfer*, 31(12):2547–2554, 1988.

[13] Adriano Milazzo. Optimization of the configuration in a CAES-TES system. *1st International Workshop - Shape and Thermodynamics*, page 12, 2008.

[14] Wm Kays and Al London. *Compact heat exchangers*. McGraw-Hill, New York, third edition, 1984.

[15] Giuseppe Grazzini and Adriano Milazzo. A thermodynamic analysis of multistage adiabatic CAES. *Proceedings of the IEEE*, 100(2):461–472, 2012.

[16] T. R. Davenne, S. D. Garvey, B. Cardenas, and M. C. Simpson. The Cold Store for a Thermal Pumping Energy Storage System. In *Offshore Energy and Storage Conference*, Valletta, 2016.

[17] Pau Farres-Antunez. Modelling of Thermal Energy Storage for Bulk Electricity Storage. Technical report, Cambridge University Engineering Department, Cambridge, 2015.

[18] P. Farres-Antunez and A. J. White. Optimization of heat exchangers operating with real fluids for termomechanical energy storage. In *Offshore Energy and Storage Conference*, Valletta, 2016.

[19] I.H. Bell, J. Wronski, S. Quoilin, and V. Lemort. Pure and pseudo-pure fluid thermophysical property evaluation and the open-source thermophysical property library coolprop. *Industrial and Engineering Chemistry Research*, 53(6):2498–2508, 2014.

[20] R. Serrano-López, J. Fradera, and S. Cuesta-López. Molten salts database for energy applications. *Chemical Engineering and Processing*, 73:87–102, 2013.

[21] Matteo Morandin, François Maréchal, Mehmet Mercangöz, and Florian Buchter. Conceptual design of a thermo-electrical energy storage system based on heat integration of thermodynamic cycles - Part A: Methodology and base case. *Energy*, 45(1):375–385, 2012.

[22] G. F. Nellis. A heat exchanger model that includes axial conduction, parasitic heat loads, and property variations. *Cryogenics*, 43(9):523–538, 2003.

[23] Juan Carlos Ordonez and Adrian Bejan. Entropy generation minimization in parallel-plates counter flow heat exchangers. *International Journal of Energy Research*, 24(August 1999):843–864, 2000.